All-atom molecular dynamics simulation of the [Fe(pyrazine)] [Ni(CN)$_4$] spin-crossover complex. I. Thermally induced spin transition in the bulk material

Shiteng Mi, Gábor Molnár ⬡, Karl Ridier ⬡, William Nicolazzi ⬡,[*] and Azzedine Bousseksou[†]
LCC, CNRS & Université de Toulouse, 205 route de Narbonne, 31077 Toulouse, France

We present an atomistic approach, based on the x-ray diffraction structure, to model cooperative spin-transition phenomena in the [Fe(pyrazine)] [Ni(CN)$_4$] spin-crossover compound. The vibronic coupling is described through a double-well potential along the totally symmetric Fe-ligand stretching mode, whereas the elastic interactions between the Fe centers are considered by an additional spin-state-dependent two-body potential. The model is then investigated through molecular dynamics simulations in the isothermal-isobaric ensemble. This approach provides a real-time spatiotemporal description of the spin transition, from the atomic movements to the nanoscale behavior, removing in this way some *ad hoc* assumptions used in state-of-the-art atomistic models, while keeping the computational cost affordable. This work is separated into two papers. In the present Part I, we report on the methodology used to describe the electron-lattice interaction to simulate the spin transition in the bulk material within a realistic molecular structure. Part II [S. Mi *et al.*, Phys. Rev. B **109**, 054104 (2024)] will address the spatiotemporal dynamics (nucleation and growth) of the spin transition in a bilayer actuator, correlating the buildup of elastic stresses and the resulting deformation of the nanoscale object using the atomistic approach developed here.

I. INTRODUCTION

In the past decades, molecular spin-crossover (SCO) materials, which exhibit a reversible transition of their electronic configuration between a low-spin (LS) and a high-spin (HS) state, have aroused extensive research interest in the field of smart, stimuli-responsive materials, with potential applications in nanoscale sensors and actuator devices [1–6]. The SCO phenomenon can be induced by a variety of external stimuli such as a temperature change, the application of pressure, an intense magnetic field, or by light irradiation. The resulting change of molecular spin-state usually generates significant modifications of many physicochemical characteristics, particularly in the optical, magnetic, dielectric, and elastic properties. In the solid state, the nature of the thermally induced SCO (gradual, abrupt, with or without hysteresis loop) mainly depends on the intermolecular interactions that exist in the material, which generate collective effects that are usually referred to under the general concept of cooperativity. It is well accepted that this cooperativity has an elastic origin, mainly attributed to the difference of the molecular volume between the two spin states [7]. Remarkably, in highly cooperative materials, the spin-state switching between the LS and HS states can take the form of a first-order spin transition with the emergence of hysteretic phenomena and associated phase separation [8]. The understanding, control, and manipulation of this bistability are crucial steps for the integration of SCO materials into technological devices [8–10].

From a theoretical point of view, the most widely employed approaches to model quasistatic spin transitions and phase transformation kinetics are microscopic models based on statistical physics, generally solved using stochastic numerical methods, such as Monte Carlo (MC) simulations. An Ising-like model was introduced by Wajnflasz [11] and then improved by Bousseksou *et al.* [12,13] to simulate the thermally induced spin transition. In this approach, the two spin states are described by fictitious scalar spin operators $\sigma = \pm 1$. Although the Ising-like model successfully reproduces first-order phase transitions and associated hysteretic phenomena, the cooperative mechanisms are introduced through a phenomenological interspin coupling, which does not explicitly consider the elastic origin of intermolecular interactions. To tackle this problem, an atom-phonon model was proposed by Nasser [14] and Nasser *et al.* [15,16]. In this approach, the description of the intramolecular part is identical to the Ising-like model, but the neighboring fictitious spins are linked by springs, modeled by harmonic potentials, with spin-state-dependent force constants $K(\sigma_i, \sigma_j)$. The atom-phonon model has been first solved for the one-dimensional case, within the mean-field approximation (variational method), leading to an effective Ising-like model, where the contributions of the lattice energy and the electron-lattice coupling are averaged and act on the fictitious spins as an effective ligand field. Afterwards, this model has been numerically studied at higher dimensions using MC simulations [17–24], which allow the deformation of the lattice. Indeed, the lattice degrees of freedom can be then considered, and the elastic strain and stress fields produced by the spin-state change can be mapped. As such, the spin transition can be analyzed both from the electronic and structural viewpoints. Based on these microscopic

*William.nicolazzi@lcc-toulouse.fr
†Azzedine.Bousseksou@lcc-toulouse.fr

elastic models, several important experimental observations have been successfully reproduced, thanks to the explicit consideration of the elastic nature of the intermolecular interactions. The nucleation and domain growth mechanisms during the spin transition have been widely addressed with this new class of models, and the phase transformation behaviors in nanoscale objects have been successfully simulated. However, giving realistic values to the model parameters, extracted from experimental data, remains impossible or at least very complicated [25] due to the drastic simplifications involved in these models.

Instead of fictitious spins, an alternative way to describe the molecular switching property is the introduction of a double-well potential [26]. This allows us to explicitly consider the inner vibrational degrees of freedom of SCO complexes, which therefore become dynamical variables. Most of the time, all these intramolecular degrees of freedom are described by an effective metal-ligand distance, which turns out to be sufficient for qualitative investigations of SCO materials. Molecular dynamics (MD) simulations and the transfer integral method [27–31] have been then used to study the cooperativity, thermal expansion, clustering mechanism, and density of vibrational states based on this type of vibronic models. The obtained results provide a qualitative explanation for the origin of the cooperativity and the mechanism of the vibrational entropy driven first-order spin transition in SCO materials. However, this approach was explored only on spring-ball structures, which makes the parametrization of the models somewhat arbitrary. Obviously, these models also ignore the details of the coordination sphere as well as the intricate crystal structure of SCO materials, which determine genuine properties of different SCO compounds.

One potential approach to model the spin transition in a realistic structure is the hybrid MC/MD method, in which the elastic MC model is used to control the spin-state switching and the MD method is then employed to control the lattice relaxation. Based on spring-ball structures, the hybrid MC/MD method has been used to investigate the HS/LS interface propagation, domain growth mechanisms, and light-induced spin-state trapping (LIESST) effects [32–36]. Remarkably, relying on the ligand-field force field (LFFF), this hybrid method was also employed to study the thermally induced spin transition in the [Fe(pyrazine)$_2$] [Pt(CN)$_4$] compound with a realistic structure as well as the effects of rotations of pyrazine ligands and guest molecules on the SCO properties [37–40]. However, it is well known that the typical time scale investigated in conventional MD simulations spans from picoseconds to microseconds, while it shifts from microseconds to milliseconds for MC simulations, provided that the time scale of these computational algorithms (based on random samplings) can be effectively related to the real time (e.g., through kinetic/diffusive MC methods) [41]. Due to these issues, it may be thus difficult to provide a reliable time evolution during the simulation.

On the other hand, the density functional theory (DFT) calculation based on quantum mechanics has become a powerful method to predict and investigate electronic and structural properties of SCO solids [42–51]. Since it remains a challenging task to handle the temperature effect and to simulate the spin-state switching using DFT methods,

ab initio MD (AIMD) simulation was employed to investigate the spin transition in the compound Fe$_2$[Nb(CN)$_8$] · (4−pyridinealdoxime)$_8$ · 2H$_2$O [52]. In this approach, DFT calculations are performed on the fly before each MD step to provide interatomic forces with increased accuracy. However, the computational time of AIMD simulations still constitutes a severe limitation.

In the interim, the simulation of the spin transition on a realistic structure using nonhybrid MD methods can also be attempted. Indeed, all-atom MD simulations have been recently used with success to study the vibrational properties of different SCO complexes [53–55]. In these studies, the force field (FF) parameters were obtained either through DFT calculations [53,54] or through comparisons with spectroscopic experiments [55]. However, the FFs were built separately for the two spin states, preventing thus the simulation of the spin-state switching process. To go further, it becomes necessary to simulate switchable materials by reproducing the effect of the vibronic coupling on the elastic deformation of realistic structures. To this aim, in this paper, inspired by previous reports of Boukheddaden *et al.* [28] and Nishino *et al.* [27,29,30], we implement a vibronic approach in our recently published FF of the [Fe(pyrazine)] [Ni(CN)$_4$] SCO complex [55], enabling us to model the spin-transition process through all-atom MD simulations.

The paper is organized as follows. First, we discuss the model and methods; we describe the implementation of the intramolecular and intermolecular double-well potentials in the modified FF. Then we show and discuss the numerical results concerning the ability of this FF, coupled with all-atom MD techniques in the isothermal-isobaric ensemble, to simulate the spatiotemporal development of the thermal spin transition in the bulk [Fe(pyrazine)] [Ni(CN)$_4$] solid.

II. COMPUTATIONAL APPROACH

A. Model and method

The studied SCO compound is the metal-organic framework [Fe(pyrazine)] [Ni(CN)$_4$] [56]. The structure of [Fe(pyrazine)] [Ni(CN)$_4$] is based on two-dimensional (2D) layers of Fe[Ni(CN)$_4$] that are bridged by pyrazine to form three-dimensional (3D) structure. Despite such structural complexity, each Fe is coordinated by six nitrogen atoms [four from Ni(CN)$_4$ group, two from pyrazine], forming nearly ideal octahedral coordination. The Fe centra form a practically ideal cubic array with similar Fe-Fe distances of ∼7 Å, both within the Fe[Ni(CN)$_4$] layers and between the layers [56]. Starting from a recent work [55], the total potential energy ($E_{\text{potential}}$) of this coordination network can be described by considering the following terms:

$$E_{\text{potential}} = E_{\text{bond}} + E_{\text{angular}} + E_{\text{dihedral}} + E_{\text{improper}} + E_{\text{nonbonding}} + E_{\text{cooperativity}}^{(i)}, \tag{1}$$

where E_{bond}, E_{angular}, E_{dihedral}, E_{improper}, and $E_{\text{nonbonding}}$ are the 2-body bonding potential, the 3-body angular potential, the 4-body dihedral potential, the 4-body improper potential, and the long-range nonbonding potential, respectively. To reproduce the cooperative effects on the spin-transition behavior of the [Fe(pyrazine)] [Ni(CN)$_4$] complex, a cooperative

TABLE I. Parameters used (equilibrium angles and force constants) for the angular, dihedral, and improper force potentials.

Equilibrium angle	Force constant (kcal mol^{-1} rad^{-2})
1. C–Ni–C (90°)	86
2. Ni–C–N (180°)	134
3. Fe–N–C (180°)	80
4. N–Fe–N (90°)	54
5. C–C–N (120°)	222
6. N–Fe–N$_{pz}$ (90°)	54
7. C–N–Fe (120°)	50
I. Ni–C–C–C/Fe–N–N–N (180°)	40
II. N–Fe–C–C (180°)	60
III. Dihedral	30
IV. N–Fe–N–N (54.74°)	150

TABLE III. Parameters used for the intramolecular and intermolecular double-well potentials.

Parameter	Value
A	2
a (kcal mol^{-1} Å^{-2})	35
b (kcal mol^{-1} Å^{-2})	8
c (Å)	0.27
d (kcal mol^{-1})	0.23
J (kcal mol^{-1})	0.09
B	Variable (0–1.4)
a_0 (kcal mol^{-1} Å^{-2})	32
b_0 (kcal mol^{-1} Å^{-2})	30
c_0 (Å)	0.49
J_0 (kcal mol^{-1})	0.3

interaction term $E_{\text{cooperativity}}^{(i)}$ ($i = 1, 2$), whose origin lies in the lattice distortions, must be added to the initial formula. Two variants of this term will be further discussed hereafter. Compared with our previous work [55], the force constants in Eq. (1) are only slightly adjusted. Notably, the introduction of a new 4-body improper potential (N–Fe–N–N) appears necessary to stabilize the FeN$_6$ octahedral structure. The resulting parameters are displayed in Tables I–III.

To include the vibronic coupling in the [Fe(pyrazine)] [Ni(CN)$_4$] structure, the harmonic Fe–N interaction used in our previous work is replaced by a double-well potential, like the ones previously proposed in Refs. [26,27]:

$$E_{\text{Fe–N}}^{\text{Double–Well}}(r)$$
$$= \frac{A}{2}\Big(d + b[c - (r - r_{\text{LS}})]^2 + a(r - r_{\text{LS}})^2$$
$$- \sqrt{4J^2 + \{d + b[c - (r - r_{\text{LS}})]^2 - a(r - r_{\text{LS}})^2\}^2}\Big),$$
$$(2)$$

where r_{LS} stands for the equilibrium Fe–N bond length. Parameters a and b are associated to the LS and HS force constants, respectively. The bond length and energy differences between the HS and LS states are characterized by the parameters c and d, respectively. Here, A is a coefficient which gives the energy scale of the vibronic coupling, and it is set to 2 under the consideration of reducing the number of parameters. Also, J is the off-diagonal element, resulting from higher-order spin-orbit coupling, which mixes the LS

TABLE II. Bond-stretching force constants and corresponding bond lengths. Fe-N bonds are modeled by a double-well potential whose parameters are reported in Table III.

Bond	Force constant (kcal mol^{-1} Å^{-2})	Bond length (Å)
N–C	2512	1.158
Ni–C	220	1.857
Fe–N (LS)	Double-well	1.944
Fe–N (HS)	Double-well	2.212
C$_{pz}$–C$_{pz}$	866	1.56
C$_{pz}$–N$_{pz}$	780	1.56

and HS harmonic potentials, as shown in Fig. 1. According to the reported crystallographic data for [Fe(pyrazine)] [Ni(CN)$_4$] [57], the equilibrium Fe–N bond lengths in the LS and HS states are set to $r_{\text{LS}} = 1.944$ Å and $r_{\text{HS}} = 2.212$ Å (see Table II), respectively, giving rise to $c = r_{\text{HS}} - r_{\text{LS}} = 0.27$ Å. Here, a, b, d, and J are then obtained through a fitting procedure according to the following criteria:

$$E_{\text{Fe–N}}^{\text{Double-Well}}(r_{\text{HS}}) - E_{\text{Fe–N}}^{\text{Double-Well}}(r_{\text{LS}}) = \Delta E_{\text{HS–LS}},$$
$$\left(\frac{d^2 E_{\text{Fe–N}}^{\text{Double-Well}}}{dr^2}\right)_{r=r_{\text{LS}}} = K_{\text{LS}},$$
$$\left(\frac{d^2 E_{\text{Fe–N}}^{\text{Double-Well}}}{dr^2}\right)_{r=r_{\text{HS}}} = K_{\text{HS}}, \qquad (3)$$
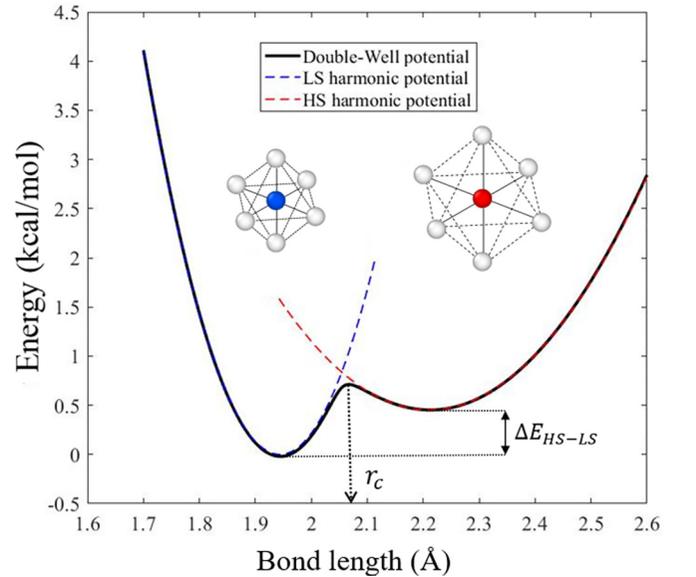
FIG. 1. Representation of the double-well potential (full black line) as well as the low-spin (LS; blue dashed line) and high-spin (HS; red dashed line) harmonic potentials as a function of the Fe–N bond length. Schematic FeN$_6$ coordination octahedra of the [Fe(pyrazine)] [Ni(CN)$_4$] complex are shown in inset, in the LS (left) and HS (right) states.

where $\Delta E_{\text{HS-LS}}$ is the energy gap between the zero-point HS and LS states, K_{LS} and K_{HS} are the force constants of the Fe–N bond in LS and HS states, respectively. Based on Raman spectroscopy data reported for [Fe(pyrazine)] [Ni(CN)$_4$] [58], the bond potential force constants can be obtained from the harmonic oscillator approximation as [59]

$$K = 4\frac{1}{N_o}\pi^2 c_l^2 \frac{m_i m_j}{m_i + m_j}\omega_e^2, \qquad (4)$$

where N_o is the Avogadro number, c_l is the velocity of light, ω_e is the harmonic frequency of the bond obtained from Raman experiments, m_i and m_j are the masses of atoms i and j, respectively. From this equation, we obtained the force constants $K_{\text{LS}} = 138$ kcal mol^{-1} Å^{-2} and $K_{\text{HS}} = 31$ kcal mol^{-1} Å^{-2}. The energy gap $\Delta E_{\text{HS-LS}} = 0.473$ kcal mol^{-1} is crudely estimated from the reported enthalpy variation (ΔH_{exp}) between two spin states by $\frac{\Delta H_{\text{exp}}}{6}$ (since each Fe site comprises six Fe–N bonds) [56]. The obtained parameters of the Fe–N double-well potential are listed in Table III. Accordingly, as shown in Fig. 1, the unstable point between the two spin states is obtained for a Fe–N bond length of $r_c = 2.07$ Å.

In Eq. (1), $E_{\text{cooperativity}}$ refers to the potential energy, which arises from the interactions between the coordination octahedra, caused by lattice distortions. For the sake of simplicity, this term is introduced in the form of a two-body potential between the nearest iron neighbors [see Fig. 2(a)]. Two different potentials have been tested. First, a monophasic Morse-like potential, like the intermolecular potential introduced in Ref. [27], has been considered [Fig. 2(b)]:

$$E_{\text{cooperativity}}^{(1)}(R) = D\{\exp[a'(R - R_0)] + \exp[-b'(R - R_0)]\}, \qquad (5)$$

where $a' = 0.5$ and $b' = 1$. Here, R_0 is a constant such that $E_{\text{cooperativity}}^{(1)}(R)$ has the minimum at $R = 7.013$ Å, corresponding to the equilibrium distance between two nearest-neighbor Fe atoms. Here, D is a tunable parameter controlling the strength of the intermolecular interactions. Secondly, a double-well (biphasic) potential using the same format than the Fe–N interaction has been proposed [Fig. 2(c)]:

$$\begin{aligned}
&E_{\text{cooperativity}}^{(2)}(R) \\
&= \frac{B}{2}\Big(b_0[c_0 - (R - R_{\text{LS}})]^2 + a_0(R - R_{\text{LS}})^2 \\
&\quad - \sqrt{4J_0^2 + \{b_0[c_0 - (R - R_{\text{LS}})]^2 - a_0(R - R_{\text{LS}})^2\}^2}\Big),
\end{aligned} \qquad (6)$$

where R_{LS} is the lattice constant of the equilibrium LS state, while B, a_0, b_0, and c_0 are parameters, which control the energy barrier between the HS and LS phases and the concavity of the double-well potential, respectively. Here, J_0 is an off-diagonal element. The term $E_{\text{cooperativity}}^{(2)}$ becomes zero for both the LS-LS and HS-HS pairs, which means that there is no excess elastic energy (induced by lattice distortion) in the pure LS and HS phases. The parameter $c_0 = 0.49$ Å is taken through the variation of lattice constants between the LS and HS forms. Here, $a_0 \approx b_0$ with the same order of magnitude as
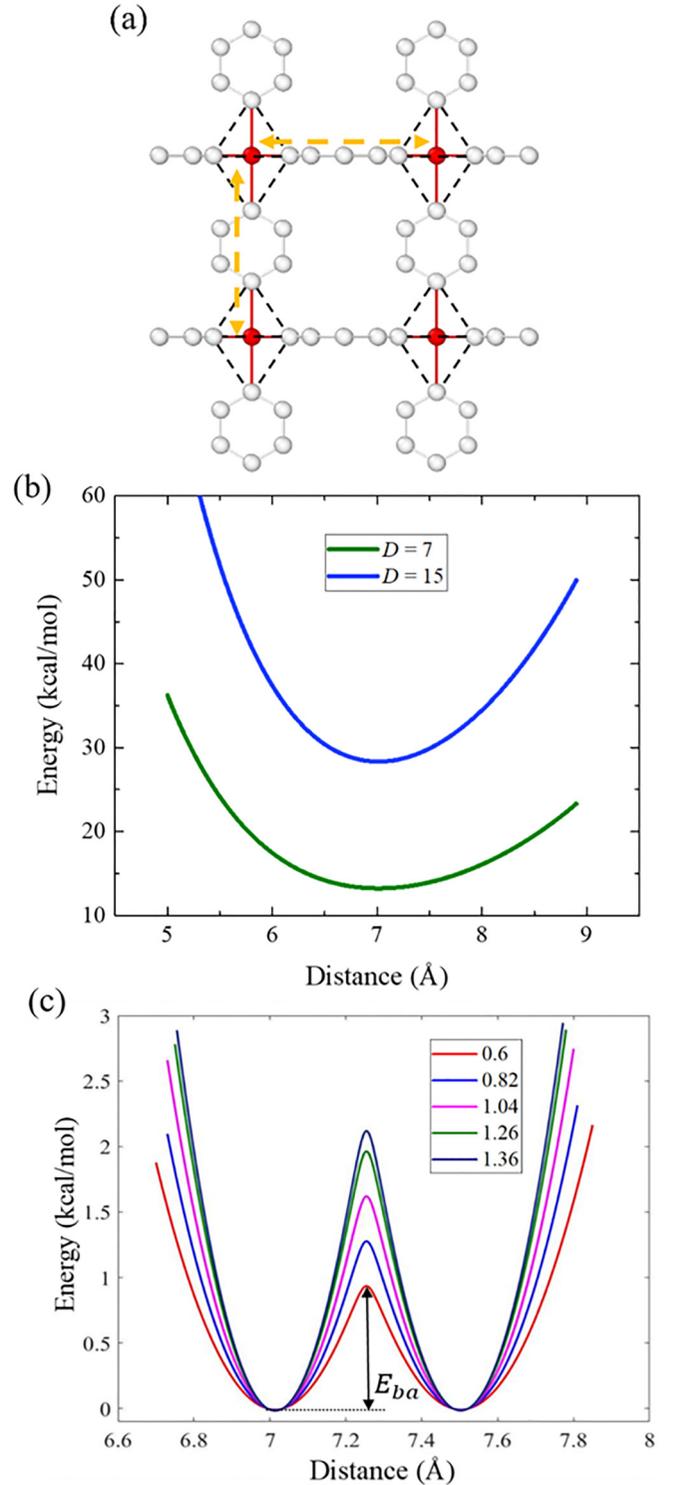
FIG. 2. (a) Schematic two-dimensional (2D) picture of the [Fe(pyrazine)] [Ni(CN)$_4$] structure, showing the Fe-Fe interactions. (b) Potential energies associated with Fe-Fe intermolecular interactions described by the monophasic potential $E_{\text{cooperativity}}^{(1)}$, given by Eq. (5), for different values of the parameter D. (c) Potential energies associated with Fe-Fe intermolecular interactions described by the double-well potential $E_{\text{cooperativity}}^{(2)}$, given by Eq. (6), for different values of the parameter B (0.6–1.36).

a was chosen to leave the energy barrier in the middle between the two minima, i.e., the maximum interaction energy appears for HS-LS pairs. Also, J_0 is chosen to be slightly larger than J to give a smooth connection between two harmonic potentials. The corresponding values of the parameters are listed in Table III.

To identify the molecular spin state, a 3D Voronoi cell was considered for each Fe site [60]. Given a metric space (M, d) and a discrete set of atomic positions $\{s_1, s_2, \ldots\} \subset M$, the Voronoi cell $V(s_i)$ associated with an atomic site s_i is the set of all points such that

$$V(s_i) = \{x \in \mathbb{R}^3 | d(x, s_i) \leqslant d(x, s_j), \ \forall i \neq j\}. \tag{7}$$

According to the above description, the shape of the Voronoi cell in the ground LS and HS states is a perfect cube. Here, the Voronoi volume associated with the Fe ions (V_{Fe}) is used as a parameter to identify the molecular spin state: if $V_{Fe} > r_c^3$, then the Fe site is in the HS state; otherwise, it is in the LS state.

B. MD simulations

The present MD simulations are carried out using the large-scale atomic/molecular massively parallel simulator (LAMMPS) software package [61]. The double-well potentials, given by Eqs. (2) and (6), are exported in an appropriate format, which could be identified by LAMMPS, by means of the Python environment. The [Fe(pyrazine)] [Ni(CN)$_4$] structure with $10 \times 10 \times 10$ unit cells is built in the LS state, which corresponds to a simulation box size of $70.13 \times 70.13 \times 70.13$ Å^3 containing 16 000 atoms. In each simulation, periodic boundary conditions are applied along the x, y, and z directions to simulate the bulk material, thus avoiding surface/interface effects. The temperature is controlled by the Nosé-Hoover thermostat [62,63], and a timestep of 1 fs is selected. The structure is initially relaxed at a temperature of $T = 50$ K for 20 000 MD steps to reach an equilibrium state. Then the system is warmed up from 50 to 460 K with increments of 10 K and then cooled back to 50 K. Here, 20 000 MD steps are selected for each temperature increment, while 5000 MD steps are used, after each increment, to stabilize the structure and measure the HS fraction. The isothermal-isobaric (NPT) ensemble is employed to control the total stress by changing the size of the simulation box along three directions. Finally, the Voronoi analysis is conducted through the Voro++ software package [64] to calculate the atomic volume of Fe sites. The spin-state configurations and atomic positions after the simulations are visualized by means of OVITO software [65].

III. RESULTS AND DISCUSSIONS

First, MD simulations have been conducted including the monophasic Morse-like potential $E_{cooperativity}^{(1)}$, given by Eq. (5), in the FF. The temperature dependence of the Fe atomic volume is plotted in Fig. 3 for different values of the parameter D. The increase of the strength of the $E_{cooperativity}^{(1)}$ leads to more gradual transitions, i.e., it is not possible to simulate a first-order transition. This result is rather unexpected because it contrasts with previous spring-ball models, where first-order
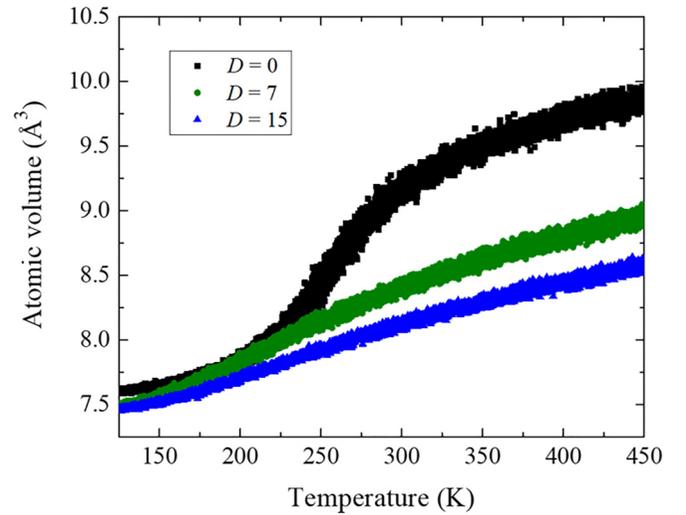
FIG. 3. Thermal evolution of the Fe atomic volume using the term $E_{cooperativity}^{(1)}$ in the force field (FF), for different values of the parameter D (strength of the intermolecular interactions).

spin transitions were successfully modeled either by increasing the elastic constant related to the intermolecular bonds or by increasing the difference between the elastic constants (or lattice parameters) of the HS and LS structures [17,18,27,66]. Here, it was not possible to simulate first-order transitions by including this spin-state-independent intermolecular potential in the FF.

Unlike spring-ball models, such as electroelastic, mechanoelastic, or anharmonic elastic models [17,20,67–69], in which the question of the structure stability does not arise and the parameters responsible for cooperative phenomena are fairly well identified, with the present model, we aim to give a more realistic description of the lattice dynamics and elastic properties of the [Fe(pyrazine)] [Ni(CN)$_4$] SCO complex. The construction of the FF and its parametrization have been achieved based on the available experimental data, while ensuring the structure stability and preserving the crystallographic properties of the material. Therefore, including the switching capability of SCO molecules into the present FF complicates this initial task. The Morse-like potential, which is simply set between two central Fe atoms, cannot describe the complexity of intermolecular interactions that may come from the N-body interactions between the ligands and local distortions in the realistic structure. An alternative way is to introduce a spin-state-dependent intermolecular two-body potential to model the elastic energy barrier that needs to be overcome to change the intermolecular distances (between two consecutive Fe centers) accompanying the spin-state switching. Here, we show that the introduction of this type of spin-state-dependent energy potential, $E_{cooperativity}^{(2)}$ given by Eq. (6), generates a local elastic energy barrier, whose effect compensates the weakness of intermolecular interactions in certain crystallographic directions. Using this double-well biphasic potential in the FF, Figs. 4(a) and 4(b) display the temperature dependence of the HS fraction (n_{HS}) and of the Fe atomic volume, respectively, upon a heating/cooling cycle, for selected values of the elastic energy barrier given by the parameter B. When $B = 0$ (zero energy barrier), the phase
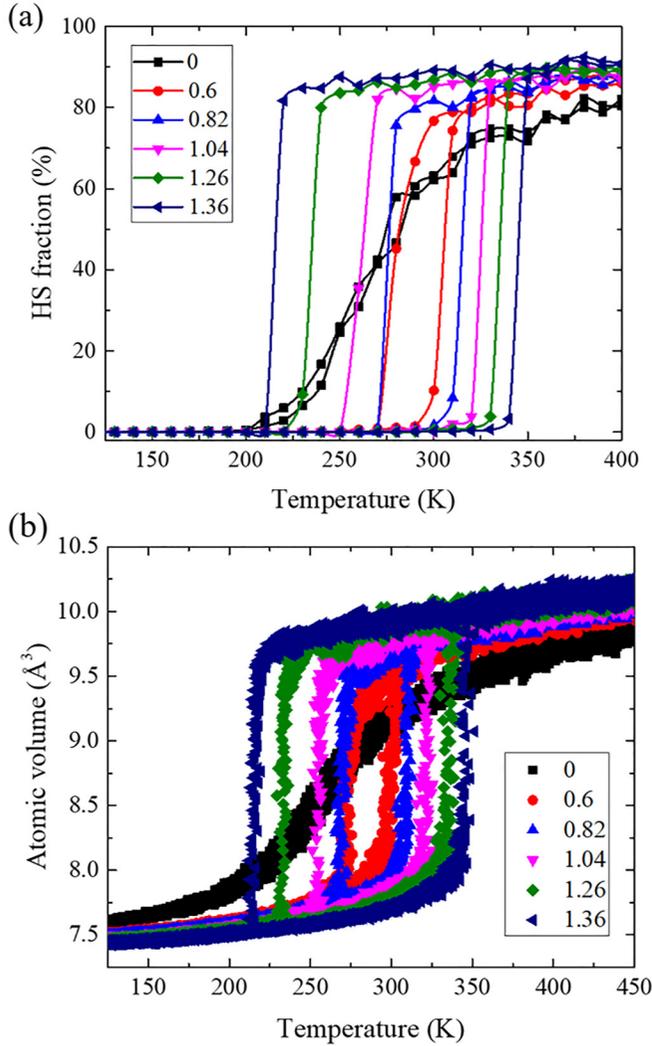
FIG. 4. Temperature dependence of (a) the high-spin (HS) fraction and (b) the atomic volume of Fe ions using the intermolecular potential $E_{\text{cooperativity}}^{(2)}$ in the force field (FF) for selected values of B (0–1.36).

transformation is found to be gradual, and a perfect overlap is observed for the thermal spin-transition curves in the heating and cooling modes [Fig. 4(a), black squared dots], as it is expected for a weakly cooperative system. Furthermore, the transition temperature T_{eq}, at which the HS and LS fractions are equal ($n_{\text{HS}} = 50\%$), is found to be $T_{\text{eq}}^{\text{MD}} \approx 280$ K.

At this point, it is interesting to note that the entropy (S) of the system can be expressed as [27]

$$S = Nk_B \left(1 - \ln \frac{\hbar}{k_B T} \sqrt{\frac{K}{m}} \right), \qquad (8)$$

where N is the number of Fe–N bonds, k_B is the Boltzmann constant, $\hbar$ is the reduced Planck constant, K is the force constant, and m is the atomic mass. Based on this expression, the entropy difference (ΔS) between the HS and LS states is

given by

$$\Delta S = S_{\text{HS}} - S_{\text{LS}} = Nk_B \ln \sqrt{\frac{K_{\text{LS}}}{K_{\text{HS}}}}, \qquad (9)$$

and the transition temperature T_{eq} is defined by the condition:

$$\Delta G = \Delta H - T_{\text{eq}} \Delta S = 0, \qquad (10)$$

where ΔG and ΔH are the Gibbs free energy difference and the enthalpy difference between the HS and LS states. Thus, the estimated transition temperature $T_{\text{eq}}^{\text{est}}$ is given by

$$T_{\text{eq}}^{\text{est}} = \frac{\Delta H}{\Delta S} = \frac{\Delta E_{\text{HS–LS}}}{k_B \ln \sqrt{\frac{K_{\text{LS}}}{K_{\text{HS}}}}}. \qquad (11)$$

According to our setting of the Fe–N potential (vide supra), the transition temperature $T_{\text{eq}}^{\text{est}} \approx 320$ K calculated by Eq. (11) is significantly higher than the value obtained from the MD simulations ($T_{\text{eq}}^{\text{MD}} \approx 280$ K). This discrepancy is certainly due to the fact that the simple thermodynamical estimation [Eq. (9)] only considers the entropy associated with the stretching vibrational modes of the Fe–N bonds which gives $\Delta S_{\text{est}} \approx 6.21N$ J K^{-1} mol^{-1}, whereas the entropy variation in the MD simulations estimated by $\Delta S_{\text{MD}} \approx \frac{N\Delta E_{\text{HS–LS}}}{T_{\text{eq}}^{\text{MD}}} = 7.07N$ J K^{-1} mol^{-1} is $\sim$12% larger than ΔS_{est}. According to the literature, the rotation of the pyrazine ligand contributes up to 9% to the total entropy [37,39,70]. The remaining contribution ($\sim$3%) comes most likely from low-frequency vibrational modes. Moreover, it should be noted that the change of spin entropy (ΔS_{spin}) coming from the difference in terms of degeneracy of spin momenta is not considered in MD simulations.

Remarkably, when increasing the value of B (i.e., the strength of the elastic interactions), we observe the occurrence of more and more abrupt SCO and the opening of a thermal hysteresis loop, characteristic of a system that exhibits a first-order transition [Figs. 4(a) and 4(b)]. As displayed in Fig. 5, the transition temperature of the system in the heating mode ($T_{1/2\uparrow}$) is progressively shifted from 280 to 350 K, while $T_{1/2\downarrow}$ (in the cooling mode) is shifted from 280 to 215 K with the increase of B from 0 to 1.4, denoting a sizeable broadening of the hysteresis loop ($\Delta T = T_{1/2\uparrow} - T_{1/2\downarrow}$) from 0 to 135 K. Importantly, we find that the equilibrium temperature between the LS and HS phases, which can be defined (as a first approximation) as

$$T_{\text{eq}} = \frac{T_{1/2\uparrow} + T_{1/2\downarrow}}{2}, \qquad (12)$$

remains virtually unchanged, regardless of the value of B [see Fig. 5(a)].

In addition to controlling the height of the elastic energy barrier, it is important to note that the parameter B also has an influence on the stiffness of the crystal lattice. Indeed, as shown in Fig. 4(b), a progressive decrease of the atomic volume is observed with B at low temperature (in the pure LS state), indicating that the lattice is less deformable in the case of higher values of B. It is also interesting to notice in Fig. 4(a) that the residual LS state observed at high temperatures decreases from $\sim$20% to $\sim$10% with the increase of
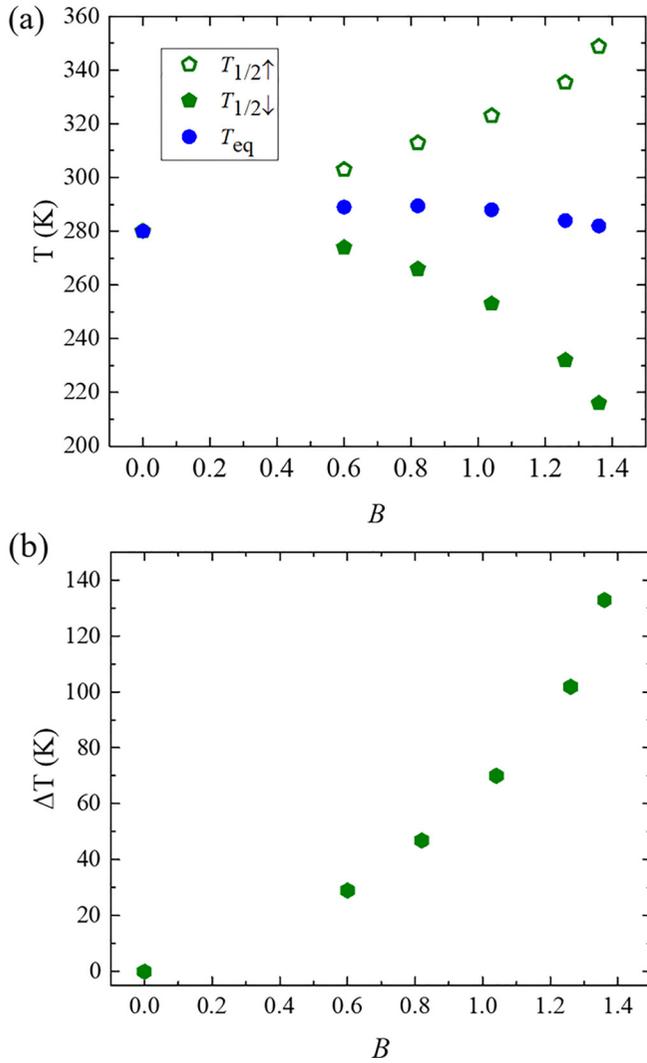
FIG. 5. Variation of (a) $T_{1/2\uparrow}$, $T_{1/2\downarrow}$, T_{eq} and (b) $\Delta T = T_{1/2\uparrow} - T_{1/2\downarrow}$ as a function of B.

B. Such an effect indicates that the elastic interaction between two Fe sites tends to stabilize the HS state at high temperature.

It is worth noting that, when $B = 0.6$, the transition temperatures upon heating and cooling are $T_{1/2\uparrow} \approx 305\,\text{K}$ and $T_{1/2\downarrow} \approx 275\,\text{K}$, respectively, giving rise to a 30-K-wide hysteresis loop, close to the experimental hysteresis width observed for the [Fe(pyrazine)] [Ni(CN)$_4$] complex ($\Delta T = 25$K) [56]. In addition, the experimentally observed transition temperature is also well reproduced, showing that our approach can simulate experimental SCO behaviors while using a realistic structure and FF.

Recently, Hochdörffer et al. [43] and Rackwitz et al. [71] introduced the notion of cooperativity energy (H_{coop}), which reflects how the spin transition of a central molecule is affected by the spin state of its neighboring molecules:

$$H_{coop} = [E_{(1HS-LS)} - E_{(LS)}] - [E_{(HS)} - E_{(1LS-HS)}], \quad (13)$$

where $E_{(LS)}$ and $E_{(HS)}$ are the energies of the system in the pure LS and HS phase, while $E_{(1HS-LS)}$ [resp. $E_{(1LS-HS)}$] is the energy of the LS (resp. HS) matrix with one molecule

in the HS (resp. LS) state. Through DFT calculations, the value of H_{coop} for the compound [Fe(pyrazine)] [Pt(CN)$_4$] was estimated to be $H_{coop} = 15\,\text{kcal mol}^{-1}$ [43]. In our MD simulations, the influence of neighboring molecules on the spin transition of a central molecule can be roughly estimated by the elastic energy barrier (E_{ba}) induced by intermolecular interactions [see Fig. 2(c)]. When $B = 0.6$, which corresponds to the experimentally observed SCO behavior, the elastic energy of the central molecule is estimated to be $6 \cdot E_{ba} = 23.5\,\text{kcal mol}^{-1}$, which is comparable with the value of $H_{coop} = 15\,\text{kcal mol}^{-1}$.

A significant advantage of the present model, which is shared with all discrete elastic models based on a deformable lattice, is the possibility to investigate the spatiotemporal aspects of the spin transition at the level of chemical bonds, by monitoring the local molecular spin state and the local structural (strain) changes as well as their time evolution upon the phase transformation. These simulations are of paramount importance to better understand the couplings between the electronic and elastic degrees of freedom in SCO materials. The present simulations make it possible to follow the temperature evolution of the spatial distribution of the fraction of HS molecules, based on the definition of the Voronoi volume associated with Fe ions. Figure 6 depicts selected snapshots of the modeled system at different temperatures during both heating and cooling (for $B = 0.6$). This viewpoint is identical to what can be obtained from other elastic models: lattice deformations are hidden, and only the local spin state is visible. In our simulations, as shown in Fig. 6, only homogeneous phase transformations are observed, and no clustering process occurs. It is also needed to mention that the clustering process cannot be observed during the spin-state switching in our simulation for lower or higher values of B (lower or higher cooperativities) due to the applied periodic boundary conditions. This result is coherent with previous theoretical investigations considering infinite systems (without surfaces), where elastic distortion mediates the interactions among local states: Spatially uniform configurations are maintained even during the first-order phase transformation [19].

In comparison with previously reported elastic models, in our approach is the possibility to simulate the real-time, spatiotemporal dynamics of the spin-state transformation in a SCO system based on a realistic structure. As an example, Fig. 7 shows sectional views of the modeled structure, along the (yOz) plane, at selected temperatures during the LS-to-HS transformation. A significant increase of the size of the system is observed concomitantly with the molecular switching, which corroborates the fact that a strong electron-lattice coupling is operating during the spin-state change. This global expansion of the system is mainly attributed to the volume increase of the FeN$_6$ coordination sphere. Indeed, as depicted in Fig. 8, an abrupt change (by ~7.5%) of the averaged Fe–N bond length is observed upon the spin transition, while in comparison, the Ni–C bond length increases only slightly (relative variation ~0.2%), in good agreement with x-ray diffraction measurements [57]. Interestingly, the progressive activation of the rotational movement of the pyrazine ligands with the temperature increase (upon the LS-to-HS transition) is also evidenced in our simulations, in good agreement with experimental observations [70]. Overall, our simulations
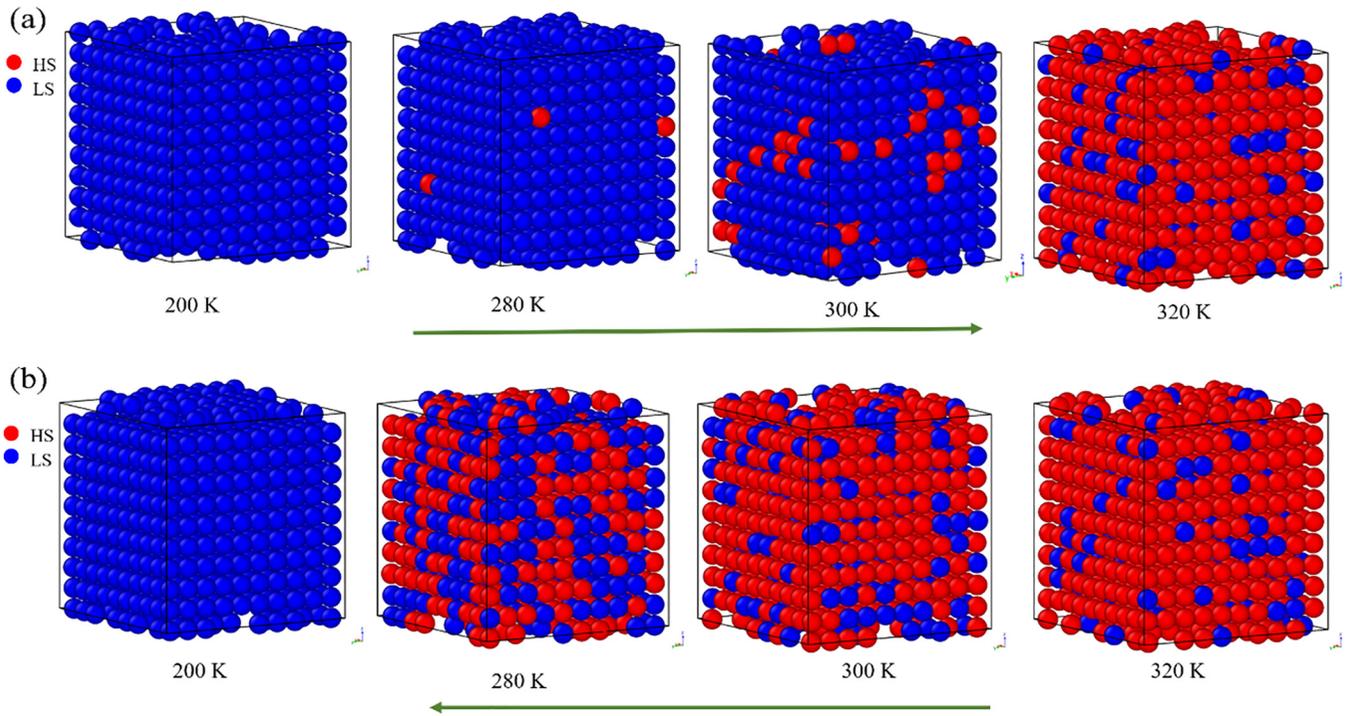
FIG. 6. Temperature dependence of the local high-spin (HS) fraction along (a) the heating process [low-spin (LS)-to-HS transition] and (b) the cooling process (HS-to-LS transition) for $B = 0.6$. In these snapshots, only the molecular spin states are depicted through blue and red balls to represent the LS and HS states, respectively. As a reminder, the transition temperatures in the heating and cooling modes are ~305 and 275 K, respectively.
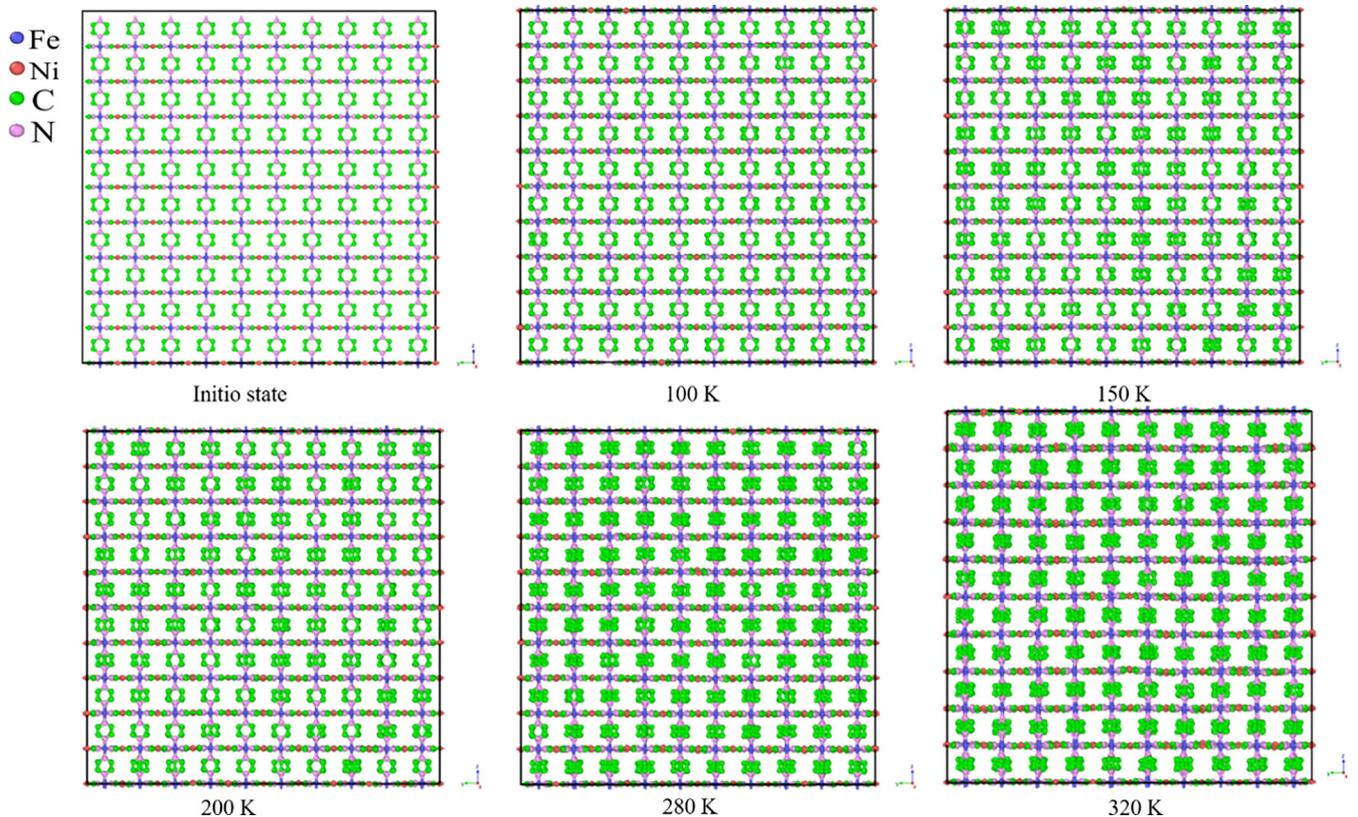
FIG. 7. Sectional view in the plane (yOz) at the middle of the simulated structure, upon the heating process at different temperatures (for $B = 0.6$). As a reminder, the transition temperature in the heating mode is $T_{1/2\uparrow} \approx 305$ K.
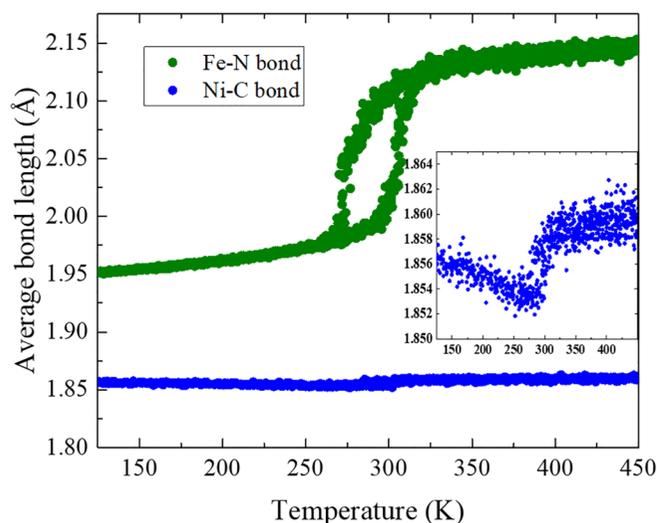
FIG. 8. Thermal evolution of the averaged Fe–N (green circles) and Ni–C (blue circles) bond lengths for $B = 0.6$. Inset: Zoom showing the thermal evolution of Ni–C bond lengths for $B = 0.6$.

allow us to perform an accurate investigation of the local and macroscopic response of a realistic structure to the electronic switching at the molecular scale, offering appealing perspectives for a deeper understanding of collective behaviors induced by elastic interactions. The analysis of the macroscopic repercussion (on the lattice) of the molecular volume change induced by the spin-state change of the compound is essential for the future elaboration of heat-to-motion devices (e.g., actuators) or for the development of more sophisticated structures such as microelectromechanical systems.

IV. CONCLUSIONS

In conclusion, an elastic model of the [Fe(pyrazine)] [Ni(CN)$_4$] SCO compound, including both intramolecular and intermolecular interactions, has been developed. We demonstrate that this model enables us to reproduce the experimentally observed thermal SCO phenomenon in [Fe(pyrazine)] [Ni(CN)$_4$], through all-atom MD simulations. The intermolecular elastic energies strongly affect the SCO behavior, and a direct correlation is observed between the width of the thermal hysteresis loop and the strength of the intermolecular elastic interaction. Compared with the widely used spring-ball models, the present model is more quantitative since it is constructed based on a realistic structure whose FF has been parametrized using available experimental data. The mechanisms of spin transition and lattice relaxation are combined during the MD simulation, which effectively avoids any time scale mismatch (that can arise when using two different simulation methods) and *ad hoc* assumptions in MC simulations. This asset is primordial to investigate the dynamical processes that arise during phase transformations, such as global deformation and interface growth. Furthermore, since the system in MC simulations is in an ideal pressure and thermal bath, the study of thermal diffusion processes in SCO materials could be an interesting direction for future MD simulations. It should be also pointed out that our approach is transferable to other SCO compounds since the FF can be parametrized by DFT even in the absence of experimental data. In addition, it is easy to open the boundary conditions of the present 3D model, which would offer the possibility to investigate the effect of surfaces/interfaces on the SCO phenomenon and, more specifically, the spatiotemporal development of the nucleation-and-growth process in cooperative SCO solids. These aspects are examined in Part II of this work for the simulation of the properties of nanoscale actuators based on the compound [Fe(pyrazine)] [Ni(CN)$_4$] [72].

[1] O. Kahn and C. J. Martinez, Spin-transition polymers: From molecular materials toward memory devices, Science **279**, 44 (1998).

[2] M. A. Halcrow, *Spin-Crossover Materials: Properties and Applications* (John Wiley & Sons, Chichester, 2013).

[3] P. Gütlich and H. A. Goodwin, *Spin Crossover in Transition Metal Compounds I* (Kluwer, Dordrecht, 1998), Vol. 1.

[4] G. Molnár, S. Rat, L. Salmon, W. Nicolazzi, and A. Bousseksou, Spin crossover nanomaterials: From fundamental concepts to devices, Adv. Mater. **30**, 1703862 (2018).

[5] K. S. Kumar and M. Ruben, Emerging trends in spin crossover (SCO) based functional materials and devices, Coord. Chem. Rev. **346**, 176 (2017).

[6] W. Nicolazzi and A. Bousseksou, Thermodynamical aspects of the spin crossover phenomenon, C. R. Chim. **21**, 1060 (2018).

[7] H. Spiering, K. Boukheddaden, J. Linares, and F. Varret, Total free energy of a spin-crossover molecular system, Phys. Rev. B **70**, 184106 (2004).

[8] K. Ridier, G. Molnár, L. Salmon, W. Nicolazzi, and A. Bousseksou, Hysteresis, nucleation and growth phenomena in spin-crossover solids, Solid State Sci. **74**, A1 (2017).

[9] E. Collet and G. Azzolina, Coupling and decoupling of spin crossover and ferroelastic distortion: Unsymmetric hysteresis loop, phase diagram, and sequence of phases, Phys. Rev. Mater. **5**, 044401 (2021).

[10] A.-I. Popa, L. Stoleriu, and C. Enachescu, Tutorial on the elastic theory of spin crossover materials, J. Appl. Phys. **129**, 131101 (2021).

[11] J. Wajnflasz, Etude de la transition "low spin"-"high spin" dans les complexes octaédriques d'ion de transition, Phys. Status Solidi B **40**, 537 (1970).

[12] A. Bousseksou, J. Nasser, J. Linares, K. Boukheddaden, and F. Varret, Ising-like model for the two-step spin-crossover, J. Phys. I **2**, 1381 (1992).

[13] A. Bousseksou, F. Varret, and J. Nasser, Ising-like model for the two step spin-crossover of binuclear molecules, J. Phys. I France **3**, 1463 (1993).

[14] J. Nasser, Diluted spin conversion compounds behaviours in the atom-phonon coupling model: Case of not too large dilution, Eur. Phys. J. B **48**, 19 (2005).

[15] J. Nasser, S. Topçu, L. Chassagne, M. Wakim, B. Bennali, J. Linares, and Y. Alayli, Two-dimensional atom-phonon coupling model for spin conversion: Role of metastable states, Eur. Phys. J. B **83**, 115 (2011).

[16] J. Nasser, K. Boukheddaden, and J. Linares, Two-step spin conversion and other effects in the atom-phonon coupling model, Eur. Phys. J. B **39**, 219 (2004).

[17] W. Nicolazzi, S. Pillet, and C. Lecomte, Two-variable anharmonic model for spin-crossover solids: A like-spin domains interpretation, Phys. Rev. B **78**, 174401 (2008).

[18] Y. Konishi, H. Tokoro, M. Nishino, and S. Miyashita, Monte Carlo simulation of pressure-induced phase transitions in spin-crossover materials, Phys. Rev. Lett. **100**, 067206 (2008).

[19] S. Miyashita, Y. Konishi, M. Nishino, H. Tokoro, and P. A. Rikvold, Realization of the mean-field universality class in spin-crossover materials, Phys. Rev. B **77**, 014105 (2008).

[20] C. Enachescu, L. Stoleriu, A. Stancu, and A. Hauser, Model for elastic relaxation phenomena in finite 2D hexagonal molecular lattices, Phys. Rev. Lett. **102**, 257204 (2009).

[21] L. Stoleriu, M. Nishino, S. Miyashita, A. Stancu, A. Hauser, and C. Enachescu, Cluster evolution in molecular three-dimensional spin-crossover systems, Phys. Rev. B **96**, 064115 (2017).

[22] C. Enachescu, M. Nishino, S. Miyashita, L. Stoleriu, and A. Stancu, Monte Carlo Metropolis study of cluster evolution in spin-crossover solids within the framework of a mechanoelastic model, Phys. Rev. B **86**, 054114 (2012).

[23] C. Enachescu, L. Stoleriu, A. Stancu, and A. Hauser, Competition between photoexcitation and relaxation in spin-crossover complexes in the frame of a mechanoelastic model, Phys. Rev. B **82**, 104114 (2010).

[24] Y. Singh, H. Oubouchou, M. Nishino, S. Miyashita, and K. Boukheddaden, Elastic-frustration-driven unusual magnetoelastic properties in a switchable core-shell spin-crossover nanostructure, Phys. Rev. B **101**, 054105 (2020).

[25] C. Enachescu and A. Hauser, Study of switching in spin transition compounds within the mechanoelastic model with realistic parameters, Phys. Chem. Chem. Phys. **18**, 20591 (2016).

[26] K. Boukheddaden, Anharmonic model for phonon-induced first-order transition in 1-D spin-crossover solids, Prog. Theor. Phys. **112**, 205 (2004).

[27] M. Nishino, K. Boukheddaden, Y. Konishi, and S. Miyashita, Simple two-dimensional model for the elastic origin of cooperativity among spin states of spin-crossover complexes, Phys. Rev. Lett. **98**, 247203 (2007).

[28] K. Boukheddaden, M. Nishino, and S. Miyashita, Molecular dynamics and transfer integral investigations of an elastic anharmonic model for phonon-induced spin crossover, Phys. Rev. Lett. **100**, 177206 (2008).

[29] M. Nishino, K. Boukheddaden, and S. Miyashita, Molecular dynamics study of thermal expansion and compression in

spin-crossover solids using a microscopic model of elastic interactions, Phys. Rev. B **79**, 012409 (2009).

[30] M. Nishino, C. Enachescu, S. Miyashita, K. Boukheddaden, and F. Varret, Intrinsic effects of the boundary condition on switching processes in effective long-range interactions originating from local structural change, Phys. Rev. B **82**, 020409 (2010).

[31] M. Nishino, C. Enachescu, S. Miyashita, P. A. Rikvold, K. Boukheddaden, and F. Varret, Macroscopic nucleation phenomena in continuum media with long-range interactions, Sci. Rep. **1**, 162 (2011).

[32] M. Nishino, T. Nakada, C. Enachescu, K. Boukheddaden, and S. Miyashita, Crossover of the roughness exponent for interface growth in systems with long-range interactions due to lattice distortion, Phys. Rev. B **88**, 094303 (2013).

[33] M. Nadeem, J. Cruddas, G. Ruzzi, and B. J. Powell, Toward high-temperature light-induced spin-state trapping in spin-crossover materials: The interplay of collective and molecular effects, J. Am. Chem. Soc. **144**, 9138 (2022).

[34] Y. Singh, K. Affes, N.-I. Belmouri, and K. Boukheddaden, Clamping of spin-crossover solid inducing crystal bending and spatial spin organization, Mater. Today Phys. **27**, 100842 (2022).

[35] N. Di Scala, N. E. I. Belmouri, M. A. P. Espejo, and K. Boukheddaden, Three-dimensional electroelastic modeling of the nucleation and propagation of the spin domains in spin-crossover materials, Phys. Rev. B **106**, 014422 (2022).

[36] M. Paez-Espejo, M. Sy, and K. Boukheddaden, Unprecedented bistability in spin-crossover solids based on the retroaction of the high spin low-spin interface with the crystal bending, J. Am. Chem. Soc. **140**, 11954 (2018).

[37] J. Cirera, V. Babin, and F. Paesani, Theoretical modeling of spin crossover in metal-organic frameworks: [Fe(pz)$_2$Pt(CN)$_4$] as a case study, Inorg. Chem. **53**, 11020 (2014).

[38] C. H. Pham, J. Cirera, and F. Paesani, Molecular mechanisms of spin crossover in the {Fe(pz)[Pt(CN)$_4$]} metal-organic framework upon water adsorption, J. Am. Chem. Soc. **138**, 6123 (2016).

[39] C. H. Pham and F. Paesani, Spin crossover in the {Fe(pz)[Pt(CN)$_4$]} metal-organic framework upon pyrazine adsorption, J. Phys. Chem. Lett. **7**, 4022 (2016).

[40] C. H. Pham and F. Paesani, Guest-dependent stabilization of the low spin state in spin-crossover metal-organic frameworks, Inorg. Chem. **57**, 9839 (2018).

[41] B. Gajdics, J. J. Tomán, and Z. Erdélyi, An effective method to calculate atomic movements in 3D objects with tuneable stochasticity (3DO-SKMF), Comput. Phys. Commun. **258**, 107609 (2021).

[42] Á. Fernández-Blanco, L. Piñeiro-López, M. Jiménez-Ruiz, S. Rols, J. A. Real, J. A. Rodríguez-Velamazán, and R. Poloni, Probing the SO$_2$ adsorption mechanism in Hofmann clathrates via inelastic neutron scattering and density functional theory calculations, J. Phys. Chem. C **126**, 8090 (2022).

[43] T. Hochdörffer, A. I. Chumakov, H.-C. Wille, V. Schünemann, and J. A. Wolny, Vibrational properties and cooperativity of the 3D spin crossover network [Fe(pyrazine)][Pt(CN)$_4$], Dalton Trans. **48**, 15625 (2019).

[44] L. H. Böttger, A. I. Chumakov, C. M. Grunert, P. Gütlich, J. Kusz, H. Paulsen, U. Ponkratz, V. Rusanov, A. X. Trautwein, and J. A. Wolny, Spin- and phase transition in the spin crossover complex [Fe(ptz)$_6$](BF$_4$)$_2$ studied by nuclear inelastic scatter-

ing of synchrotron radiation and by DFT calculations, Chem. Phys. Lett. **429**, 189 (2006).

[45] J. A. Wolny, I. Faus, J. Marx, R. Rüffer, A. I. Chumakov, K. Schlage, H.-C. Wille, and V. Schünemann, Vibrational coupling of nearest neighbors in 1-D spin crossover polymers of rigid bridging ligands. A nuclear inelastic scattering and DFT study, Magnetochemistry **2**, 19 (2016).

[46] N. O. Moussa, E. Trzop, S. Mouri, S. Zein, G. Molnár, A. B. Gaspar, E. Collet, M. Buron-Le Cointe, J. A. Real, S. Borshch *et al.*, Wavelength selective light-induced magnetic effects in the binuclear spin crossover compound {[Fe(bt)(NCS)$_2$]$_2$(bpym)}, Phys. Rev. B **75**, 054101 (2007).

[47] S. Lebègue, S. Pillet, and J. Ángyán, Modeling spin-crossover compounds by periodic DFT+U approach, Phys. Rev. B **78**, 024433 (2008).

[48] V. Meded, A. Bagrets, K. Fink, R. Chandrasekar, M. Ruben, F. Evers, A. Bernand-Mantel, J. Seldenthuis, A. Beukman, and H. Van Der Zant, Electrical control over the Fe(II) spin crossover in a single molecule: Theory and experiment, Phys. Rev. B **83**, 245415 (2011).

[49] S. Gueddida and M. Alouani, Spin crossover in a single Fe(phen)$_2$(NCS)$_2$ molecule adsorbed onto metallic substrates: An *ab initio* calculation, Phys. Rev. B **87**, 144413 (2013).

[50] G. Privault, J.-Y. Mevellec, M. Lorenc, B. Humbert, E. Janod, N. Daro, G. Chastanet, A. Subedi, and E. Collet, Symmetry-resolved study of lattice vibration and libration modes in [Fe(phen)$_2$(NCS)$_2$] crystal, Cryst. Growth Des. **22**, 5100 (2022).

[51] M. L. Marcondes, F. Zheng, and R. M. Wentzcovitch, Phonon dispersion throughout the iron spin crossover in ferropericlase, Phys. Rev. B **102**, 104112 (2020).

[52] K. Tarafder, S. Kanungo, P. M. Oppeneer, and T. Saha-Dasgupta, Pressure and temperature control of spin-switchable metal-organic coordination polymers from *abinitio* calculations, Phys. Rev. Lett. **109**, 077203 (2012).

[53] J. Herz, R. Meyer, J. A. Wolny, V. Schünemann, and H. M. Urbassek, Crystal effects in the vibrational spectra of one-dimensional molecular spin crossover crystals using molecular dynamics simulations, Appl. Phys. A **129**, 345 (2023).

[54] R. Meyer, C. Mücksch, J. A. Wolny, V. Schünemann, and H. M. Urbassek, Atomistic simulations of spin-switch dynamics in multinuclear chain-like triazole spin-crossover molecules, Chem. Phys. Lett. **733**, 136666 (2019).

[55] S. Mi, A. Fahs, G. Molnár, W. Nicolazzi, and A. Bousseksou, Molecular mechanics simulations of lattice dynamical properties of the spin crossover complex [Fe(pyrazine)] [Ni(CN)$_4$], Chem. Phys. Lett. **811**, 140232 (2023).

[56] V. Niel, J. M. Martinez-Agudo, M. C. Munoz, A. B. Gaspar, and J. A. Real, Cooperative spin crossover behavior in cyanide-bridged Fe(II)−*M*(II) bimetallic 3D Hofmann-like networks (*M* = Ni, Pd, and Pt), Inorg. Chem. **40**, 3838 (2001).

[57] P. D. Southon, L. Liu, E. A. Fellows, D. J. Price, G. J. Halder, K. W. Chapman, B. Moubaraki, K. S. Murray, J.-F. Létard, and C. J. Kepert, Dynamic interplay between spin-crossover and host-guest function in a nanoporous metal-organic framework material, J. Am. Chem. Soc. **131**, 10998 (2009).

[58] G. Molnár, V. Niel, A. B. Gaspar, J. A. Real, A. Zwick, A. Bousseksou, and J. J. McGarvey, Vibrational spectroscopy of cyanide-bridged, iron(II) spin-crossover coordination polymers: Estimation of vibrational contributions to the entropy change associated with the spin transition, J. Phys. Chem. B **106**, 9701 (2002).

[59] V. Morozov, V. Belokopytov, G. Zegzhda, and V. Moiseenko, Force constants and vibration frequencies and forms of the coordination center of cysteine-containing chromium (III) trischelates, Found. Phys. Lett. **15**, 508 (2002).

[60] G. Voronoi, New applications of continuum parameters to theory of quadratic forms, J. Fur Reine Angew. **1908**, 198 (1908).

[61] S. Plimpton, Fast parallel algorithms for short-range molecular dynamics, J. Comput. Phys. **117**, 1 (1995).

[62] S. Nosé, A unified formulation of the constant temperature molecular dynamics methods, J. Chem. Phys. **81**, 511 (1984).

[63] W. G. Hoover, Canonical dynamics: Equilibrium phase-space distributions, Phys. Rev. A **31**, 1695 (1985).

[64] C. Rycroft, *Voro++: A three-dimensional Voronoi cell library in C++* (Lawrence Berkeley National Lab, Berkeley, 2009).

[65] A. Stukowski, Visualization and analysis of atomistic simulation data with OVITO—The open visualization tool, Model. Simul. Mater. Sci. Eng. **18**, 015012 (2009).

[66] C. Cantin, J. Kliava, A. Marbeuf, and D. Mikaïlitchenko, Cooperativity in a spin transition ferrous polymer: Interacting domain model, thermodynamic, optical and EPR study, Eur. Phys. J. B **12**, 525 (1999).

[67] K. Boukheddaden, I. Shteto, B. Hôo, and F. Varret, Dynamical model for spin-crossover solids. I. Relaxation effects in the mean-field approach, Phys. Rev. B **62**, 14796 (2000).

[68] A. Slimani, K. Boukheddaden, F. Varret, H. Oubouchou, M. Nishino, and S. Miyashita, Microscopic spin-distortion model for switchable molecular solids: Spatiotemporal study of the deformation field and local stress at the thermal spin transition, Phys. Rev. B **87**, 014111 (2013).

[69] A. Slimani, K. Boukheddaden, and K. Yamashita, Thermal spin transition of circularly shaped nanoparticles in a core-shell structure investigated with an electroelastic model, Phys. Rev. B **89**, 214109 (2014).

[70] J. A. Rodríguez-Velamazán, M. A. González, J. A. Real, M. Castro, M. C. Muñoz, A. B. Gaspar, R. Ohtani, M. Ohba, K. Yoneda, Y. Hijikata *et al.*, A switchable molecular rotator: Neutron spectroscopy study on a polymeric spin-crossover compound, J. Am. Chem. Soc. **134**, 5083 (2012).

[71] S. Rackwitz, W. Klopper, V. Schünemann, and J. A. Wolny, Quantification of intramolecular cooperativity in polynuclear spin crossover Fe(II) complexes by density functional theory calculations, Phys. Chem. Chem. Phys. **15**, 15450 (2013).

[72] S. Mi, G. Molnár, K. Ridier, W. Nicolazzi, and A. Bousseksou, following paper, All-atom molecular dynamics simulation of the [Fe(pyrazine)][Ni(CN)$_4$] spin-crossover complex. II. Spatiotemporal study of a bimorph actuator, Phys. Rev. B **109**, 054104 (2024).